Advances in Materials Research, *Vol. 14, No. 3 (2025) 205-229*
https://doi.org/10.12989/amr.2025.14.3.205

Impact of partial loads on elastic bending behavior of functionally graded plates resting on a partial elastic foundation

Mounir Takouachet[1b], Abderrahmane Menasria[2,4a], Nabil Himeur[3a], Abdelhakim Bouhadra[*2,4] and Abdelouahed Tounsi[4,5a]

[1]*Civil Engineering Department, Faculty of Technology, University of Sidi Bel Abbes, BP 89, Sidi Bel Abbes 22000, Algeria*
[2]*Civil Engineering Department, Faculty of Sciences and Technology, University of Khenchela, BP 1252 Road of Batna, Khenchela 40000, Algeria*
[3]*Mechanical Engineering Department, Faculty of Sciences and Technology, University of Khenchela, BP 1252 Road of Batna, Khenchela 40000, Algeria*
[4]*Materials and Hydrology Laboratory, University of Sidi Bel Abbes, BP 89, Sidi Bel Abbes 22000, Algeria*
[5]*Department of Civil and Environmental Engineering, King Fahd University of Petroleum & Minerals, 31261 Dhahran, Eastern Province, Saudi Arabia*

(*Received January 17, 2025, Revised April 10, 2025, Accepted April 21, 2025*)

Abstract. This study investigates the coupled effects of loading types, thickness stretching, Winkler–Pasternak and Kerr foundation variations on the flexural behaviour of simply supported functionally graded (FG) plates. A simplified quasi-3D high-order shear deformation theory incorporating integral terms is used. The governing equilibrium equations consider the interaction between the loading type and the variation of Winkler–Pasternak and Kerr foundation parameters. The numerical results for non-dimensional stresses and displacements are obtained using the virtual displacement principle and Navier's solution technique. The accuracy of the non-dimensional formulas is validated against existing literature, demonstrating excellent agreement. Additionally, several parametric studies examine the effects of various geometric and material factors. This analytical model is well suited for analyzing the bending behaviour of simply supported FG plates in specific engineering applications.

Keywords: elastic bending; FG Plate; Navier solution; partial foundation; partial loads; Quasi-3D theory; virtual work principle

1. Introduction

Functionally graded materials (FGMs) are materials whose mechanical properties vary continuously with position, and the material properties are graded in compositions to optimize the materials for a desired application. Due to the ability to have differing mechanical properties based on the position in the material, FGMs have advantages in structural materials where optimal

*Corresponding author, Ph.D., Professor., E-mail: bouhadrahako@gmail.com
[a] Ph.D.
[b] Ph.D. Student

http://www.techno-press.org/?journal=amr&subpage=5 ISSN: 2234-0912 (Print), 2234-179X (Online)

mechanical behaviour is desired. FGMs have been widely used for applications in mechanical design, materials for thermal barrier coatings, biomedical applications, nontoxic materials in nuclear support applications, etc. Recent advancements in contact mechanics and dynamic behavior of advanced materials demonstrate significant interdisciplinary progress through integrated analytical, numerical, and machine learning approaches. Functionally graded materials (FGMs) exhibit tailored stress distributions under mechanical loads, with analytical models revealing critical separation loads and inhomogeneity effects on contact pressures; Yaylacı *et al*. (2024).

Concurrently, Euler–Bernoulli nanobeams under thermo-magneto-mechanical loads show nonlinear frequency-amplitude dependencies, addressed via nonlocal continuum theory and homotopy perturbation methods, Adıyaman *et al*. (2023). Multiscale modeling of composite shells in hygrothermal environments highlights synergistic effects of curvature and magnetic fields on nonlinear wave propagation; Selvamani *et al*. (2024), while orthotropic layer analyses validate finite element (FEA) and multilayer perceptron (MLP) methods for contact stress prediction, achieving <5% error rates; Selvamani *et al*. (2024).

Friction stir processing enhances shipbuilding steels' strength (e.g., AH-32) with minimal formability loss, demonstrated through experimental-FEA-ANN correlations Sekban *et al*. (2024; Yaylacı *et al*. (2024). Nano-patterned surfaces' mechano-bactericidal efficacy is quantified via FEM, showing peak sharpness and spacing critically influence bacterial cell deformation, Sekban *et al*. (2024; Yaylaci *et al*. (2023). Cyclic ratcheting studies on beams propose frequency-dependent failure criteria using elastic-plastic models; Sekban *et al*. (2024), while crack propagation in FG layers under thermal gradients is analyzed via FEM and ANN, correlating stress intensity factors with material gradation; Fuyad *et al*. (2024).

Collectively, these works underscore the convergence of theoretical rigor employing integral transforms, Reddy's third-order shear deformation, and Hamilton's principles Öner *et al*. (2024); Rajendran *et al*. (2024); with computational validation, advancing design paradigms for aerospace, marine, and biomedical systems. Persistent challenges include scaling inhomogeneous material models and optimizing process-induced anisotropies in smart composites. Tran *et al*. (2020) developed an innovative method known as the edge-based smoothed finite element method, featuring the mixed interpolation of tensorial components. This enhanced technique is designed to analyze bending and dynamic behavior. The experimentation is conducted using Halpin-Tsai mixture rules. Pham *et al*. (2023) studied the elastic bending and dynamic analysis of functionally graded porous nanobeams through a finite element formulation based on Eringen's theory and refined higher-order deformation plate theory, which is endowed with a new shape function. Nguyen *et al*. (2023) investigated the dynamic characteristics of porous bidirectional FG nanobeams in a hygrothermal environment on an elastic foundation, employing Eringen's theory and the finite element method. Nguyen and Pham (2023) introduced a novel C1 rectangular element based on Shi's third-order shear deformation theory (TSDT) for analyzing the bending and vibration of FG sandwich plates. This method utilizes a quadrilateral element with four nodes, each having seven degrees of freedom. Additionally, Pham *et al*. (2023) elaborated a finite element formulation based on nonlocal theory to study the dynamic response of viscoelastic orthotropic plates resting on a variable viscoelastic foundation, considering the mechanical properties of the material according to Kelvin's model. In further research, Pham *et al*. (2023) coupled the edge-based smoothed finite element method (ES-FEM) with the mixed interpolation of tensorial components triangular (MITC3) element to examine the vibration of sandwich plates featuring a functionally graded porous (FGP) core under blast loading. The governing differential equations were solved using the Newmark-beta method. Pham and Nguyen (2022) investigated the elastic bending and dynamic

response of functionally graded porous nanobeams utilizing an advanced finite element formulation based on Eringen's theory and refined higher-order deformation plate theory, employing a new shape function.

Various analytical methods have been employed in the engineering fields mentioned above to evaluate the bending behavior of these components. Slimani *et al*. (2024) investigated a quasi-three-dimensional (3D) refinement using a novel higher-order shear deformation theory to assess static bending with two types of porous porosity distribution. Khadraoui *et al*. (2022) explored the impact of thickness stretching and nonlinear hygro-thermo-mechanical loading on the bending behavior of functionally graded (FG) beams. Young's modulus, thermal expansion, and moisture concentration coefficients were assumed to change gradually and continuously according to a power-law distribution concerning the volume fractions of the constituent materials. Furthermore, the governing equilibrium equations considered the interaction between the thermal, mechanical, and moisture loads. Meski *et al*. (2024) conducted a study on the nonlinear hygro-thermo-mechanical coupling loading (NL-HTMCL) of functionally graded sandwich beams (FGSBs). The study considered various symmetric and asymmetric beam configurations with FGSB skins. A novel quasi-3D high shear deformation theory was utilized to analyze the behavior of these multi-type sandwich beams. Li *et al*. (2024) developed analytical expressions for the bending solutions of a simply supported rectangular functionally graded material (FGM) plate using a four-variable refined higher-order shear deformation theory. These solutions were demonstrated to be directly related to the corresponding solutions of a homogeneous Kirchhoff plate under classical plate theory. The deflection, stress components, resultant forces, and bending moments of the thick FGM plate were analytically expressed in terms of the deflection of the reference homogeneous Kirchhoff plate with identical geometry, loading conditions, and boundary conditions. Moreover, additional researchers have focused their attention on various structural bending issues (Houari *et al*. 2003, Yushan and Zhen 2024, Huang *et al*. 2023, Chitour *et al*. 2022).

Elastic foundation-supported plates are widely used in various structural applications, including aircraft runways, deep wells, bridges, and buildings. The simplest model for such foundations is the Winkler model (Wu *et al*. 2011), which represents the foundation as a series of independent springs without interaction. Pasternak extended the Winkler model by introducing a shear layer between the springs, resulting in a two-parameter model. This approach is commonly referred to as the Pasternak foundation model (Yaghoobi and Fereidoon 2014). Do *et al*. (2024) conducted a nonlinear static bending analysis of functionally graded porous sandwich plates with a ceramic core (FSCC). The FSCC plates were assumed to rest on a Kerr foundation and were subjected to a transverse uniform load. The analysis utilized the mixed interpolation of tensorial components for the four-node rectangular element (MITC4). Kumar *et al*. (2024) developed an analytical solution for the bending analysis of functionally graded porous sandwich plates, both with and without holes, supported by elastic foundations. The analysis employed the first-order shear deformation theory within a finite element method framework. Hoang *et al*. (2023) developed a novel theoretical model to analyze the effects of an arbitrarily distributed Kerr foundation on the free vibration and transient responses of functionally graded material plates in a thermal environment. The mechanical properties of the FGM plates were assumed to vary with plate thickness according to a power law distribution. The three-parameter Kerr model was based on the independence of the upper and lower elastic layers from the shear layer. The shape and location of the elastic foundation were defined arbitrarily using mathematical functions. Tamrabet *et al*. (2023) investigated the influence of porosity on the buckling behavior of thick functionally graded sandwich plates. The plates were subjected to various in-plane loads and supported by different boundary conditions. A newly developed sandwich plate theory

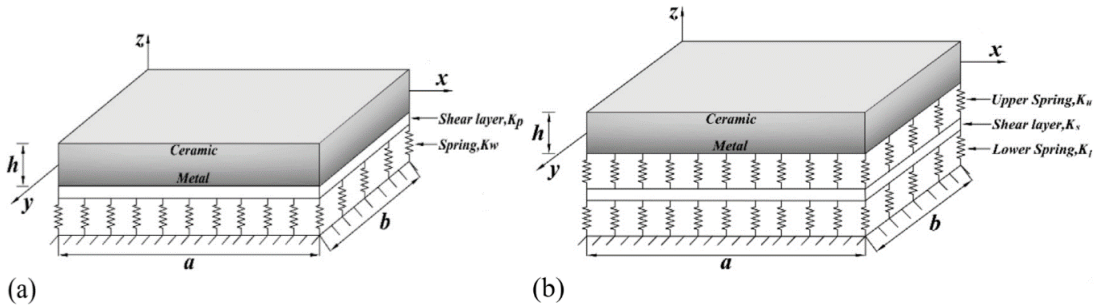

Fig. 1 The geometry of rectangular FGM plate resting on (a) Winkler-Pasternak foundation, and (b) Kerr foundation

that incorporates a modified power law function for both symmetric and asymmetric configurations was used in the formulation. Other exciting studies have focused on the bending analysis of composite structures supported by various types of elastic foundations (Chitour *et al*. 2022, Hoang *et al*. 2024, Soltani *et al*. 2024, Salehipour *et al*. 2024, Rachid *et al*. 2022, Han and Liew 1997, Thai *et al*. 2013, Nebab *et al*. 2019, Park and Choi 2018, Zenkour *et al*. 2014, Ameur *et al*. 2011).

This study investigates the combined influence of variable Winkler–Pasternak and Kerr foundations on the bending behavior of functionally graded (FG) plates. A key objective is to examine the plate response under various loading conditions. Himeur *et al*. (2022) proposed a novel quasi-3D theory to analyze the coupled effects of variable Winkler–Pasternak foundations on functionally graded (FG) plates. The theory considers the simultaneous variation of both parameters of the Winkler–Pasternak foundation while the FG plates are subjected to different loading conditions.

Based on a comprehensive literature review and the authors' knowledge, very little existing research has explored the combined effects of non-uniform Winkler–Pasternak and Kerr foundations, along with different types of loading, on the bending behavior of functionally graded (FG) plates using quasi-3D theories. This quasi-3D theory, utilizing integral terms, examines the effects of variable Winkler–Pasternak and Kerr foundations on the bending behavior of functionally graded (FG) plates under various loading conditions. The Navier solution technique, which employs a double Fourier series and satisfies the boundary conditions of a simply supported plate, is employed to solve the resulting equilibrium equations. The study considers the impacts of thickness stretching, power-law index, side-to-thickness ratio, plate aspect ratio, load type, and Winkler–Pasternak and Kerr foundation parameters on the bending behavior. The key feature of this study is the use of undetermined integral terms in kinematics, incorporating the stretching effect to simulate 3D reality more accurately. Firstly, the foundational behavior is approximated using the Kerr model, which accounts for the influence of geometry on the behavior of the FGM plate. Secondly, various partial loads are considered to analyze the plate's response to different loading conditions. Moreover, our analytical model simplifies the problem by reducing the number of unknowns to four variables, making it more efficient than alternative models.

2. Mathematical formulation

A simply supported FGM plate with length a, width b, and thickness h rests on an elastic foundation. The x, y, and z coordinates are defined according to the length, width, and thickness, as

shown in Fig. 1. Moreover, the material properties vary smoothly and continuously across the thickness of the FGM face sheets.

The Voigt mixing rule can express the effective properties of the material, such as Young's modulus E, Poisson's ratio υ, and mass density ρ. Based on the thick plate integral model and satisfying the requirements for transverse shear stresses and deformations, which vanish at the upper and lower sides of the plate (z=±h/2), the following displacement field of the plate can be used as Zaoui *et al*. (2019):

$$\begin{aligned} u(x,y,z) &= u_0(x,y) - z\frac{\partial w_0}{\partial x} + k_1 f(z)\int \theta(x,y)\,dx \\ v(x,y,z) &= v_0(x,y) - z\frac{\partial w_0}{\partial y} + k_2 f(z)\int \theta(x,y)\,dy \\ w(x,y,z) &= w_0(x,y) + g(z)\phi_z(x,y) \end{aligned} \tag{1}$$

where: $u_0, v_0, w_0, \theta \; and \; \phi_z$ are defined as the median plane, five unknown displacements of the plate, and $k_1 = \alpha^2 \; and \; k_2 = \beta^2$. The coefficient. $k_1 \; and \; k_2$ are related to the plate's geometry. The displacement field implies only five unknowns when considering the thickness stretching effect.

The simplified function shape $f(z)$ and $g(z)$ are given in the following form

$$f(z) = sin\left(z - \frac{3z^4}{4}\right) \quad and \quad g(z) = \frac{df(z)}{dz} \tag{2}$$

The relationships between strains and displacements, derived from the displacement field, are expressed in the following compact form.

$$\begin{aligned} &\begin{Bmatrix}\varepsilon_x \\ \varepsilon_y \\ \gamma_{xy}\end{Bmatrix} = \begin{Bmatrix}\varepsilon_x^0 \\ \varepsilon_y^0 \\ \gamma_{xy}^0\end{Bmatrix} + z\begin{Bmatrix}k_x^b \\ k_y^b \\ k_{xy}^b\end{Bmatrix} + f(z)\begin{Bmatrix}k_x^s \\ k_y^s \\ k_{xy}^s\end{Bmatrix}, \\ &\begin{Bmatrix}\gamma_{yz} \\ \gamma_{xz}\end{Bmatrix} = f'(z)\begin{Bmatrix}\gamma_{yz}^0 \\ \gamma_{xz}^0\end{Bmatrix} + g(z)\begin{Bmatrix}\gamma_{yz}^1 \\ \gamma_{xz}^1\end{Bmatrix}, \\ &\varepsilon_z = g'(z)\,\varepsilon_z^0 \end{aligned} \tag{3}$$

where

$$\begin{Bmatrix}\varepsilon_x^0 \\ \varepsilon_y^0 \\ \gamma_{xy}^0\end{Bmatrix} = \begin{Bmatrix}\dfrac{\partial u_0}{\partial x} \\ \dfrac{\partial v_0}{\partial y} \\ \dfrac{\partial u_0}{\partial y} + \dfrac{\partial v_0}{\partial x}\end{Bmatrix}, \qquad \begin{Bmatrix}k_x^b \\ k_y^b \\ k_{xy}^b\end{Bmatrix} = \begin{Bmatrix}-\dfrac{\partial^2 w_0}{\partial x^2} \\ -\dfrac{\partial^2 w_0}{\partial y^2} \\ -2\dfrac{\partial^2 w_0}{\partial x \partial y}\end{Bmatrix} \tag{4}$$

$$\begin{Bmatrix}k_x^s \\ k_y^s \\ k_{xy}^s\end{Bmatrix} = \begin{Bmatrix}k_1\theta \\ k_2\theta \\ k_1\dfrac{\partial}{\partial y}\int \theta\,dx + k_2\dfrac{\partial}{\partial x}\int \theta\,dy\end{Bmatrix}, \qquad \begin{Bmatrix}\gamma_{yz}^0 \\ \gamma_{xz}^0\end{Bmatrix} = \begin{Bmatrix}k_2\int \theta\,dy \\ k_1\int \theta\,dx\end{Bmatrix}, \varepsilon_z^0 = \phi_z \tag{5}$$

The terms referred to as integral in the previous formulation are addressed by the de Navier method and may be presented as indicated.

$$\frac{\partial}{\partial y}\int \theta\, dx = A'\frac{\partial^2\theta}{\partial x\partial y}, \qquad \frac{\partial}{\partial x}\int \theta\, dy = B'\frac{\partial^2\theta}{\partial x\partial y} \tag{6}$$

The coefficients A' and B' are written based on the Navier solution. Therefore, A', B', k_1 and k_2 as follows

$$A' = -\frac{1}{\alpha^2}, \qquad B' = -\frac{1}{\beta^2}, \qquad k_1 = \alpha^2, \qquad k_2 = \beta^2 \tag{7}$$

where α and β are defined by

$$\alpha = m\pi/a and \beta = n\pi/b \tag{8}$$

2.1 Constitutive relations

The linear behavioral relationships of an FG plate as a function of 3D elasticity are written as

$$\begin{Bmatrix}\sigma_x\\ \sigma_y\\ \sigma_z\\ \tau_{yz}\\ \tau_{xz}\\ \tau_{xy}\end{Bmatrix} = \begin{bmatrix}C_{11} & C_{12} & C_{13} & 0 & 0 & 0\\ C_{12} & C_{22} & C_{23} & 0 & 0 & 0\\ C_{13} & C_{23} & C_{33} & 0 & 0 & 0\\ 0 & 0 & 0 & C_{66} & & \\ 0 & 0 & 0 & & C_{55} & \\ 0 & 0 & 0 & & & C_{44}\end{bmatrix}\begin{Bmatrix}\varepsilon_x\\ \varepsilon_y\\ \varepsilon_z\\ \gamma_{xy}\\ \gamma_{yz}\\ \gamma_{xz}\end{Bmatrix} \tag{9}$$

The C_{ij} $(i,j = 1,2,4,5,6)$ are given in terms of engineering constants as follow

$$\begin{aligned} C_{ii} &= \frac{(1-\nu)E(z)}{(1-\nu)(1-2\nu)} \quad if \quad (i = 1,2,3).\\ C_{ij} &= \frac{\nu E(z)}{(1-\nu)(1-2\nu)} \quad if\ (i,j = 1,2,3).\\ C_{ii} &= \frac{E(z)}{2(1+\nu)} \quad if \quad (i = 4,5,6). \end{aligned} \tag{10}$$

2.2 Equations of equilibrium

The theory of virtual displacements is used to determine the governing equations of the equilibrium state. In the instant case, the principle of virtual is expressed as

$$\int_V \delta U + \delta V + \delta U_R = 0 \tag{11}$$

where: δU, δV and δU_R are respectively representing the variations of strain energy, the potential energy of the applied loads, and the potential energy of the foundation.

The strain energy variation of the FG plate is obtained by

$$\begin{aligned} \delta U = \int_A [&N_x\delta\varepsilon_x^0 + N_y\delta\varepsilon_y^0 + N_z\delta\varepsilon_z^0 + N_{xy}\delta\gamma_{xy}^0 + M_x^b\delta k_x^b + M_y^b\delta k_y^b\\ &+M_{xy}^b\delta k_{xy}^b + M_x^s\delta k_x^s + M_y^s\delta k_y^s + M_{xy}^s\delta k_{xy}^s + S_{yz}^S\delta\gamma_{yz} + S_{xz}^S\delta\gamma_{xz}]dA = 0 \end{aligned} \tag{12}$$

where A represents the plane section, and N, M, Q, and S are, respectively, in-plane force resultants, moment resultants, and transverse shear stress resultants; the following formulas determine all of those

$$\begin{Bmatrix} N_x & N_y & N_{xy} \\ M_x^b & M_y^b & M_{xy}^b \\ M_x^s & M_y^s & M_{xy}^s \end{Bmatrix} = \int_{-h/2}^{h/2} (\sigma_x, \sigma_y, \tau_{xy}) \begin{Bmatrix} 1 \\ z \\ f(z) \end{Bmatrix} dz \tag{13a}$$

$$N_z = \int_{-h/2}^{h/2} \sigma_z \, \mathrm{g}'(z) \; dz \tag{13b}$$

$$(S_{xz}^s, S_{yz}^s) = \int_{-h/2}^{h/2} (\tau_{xz}, \tau_{yz}) \, \mathrm{g}(z) \; dz \tag{13c}$$

The expression of the variation of the applied load potential energy can be written as

$$\delta V = -\int_A q\delta \left(w_0(x,y) + g(z)\phi_z(x,y)\right) dA \tag{14}$$

Also, elastic foundation potential energy variation can be annotated as

$$\delta U_R = \int \left(f_e^{Pasternak} + f_e^{kerr}\right) \delta w dA \tag{15}$$

Fe is the density of the reaction force of the foundation. For the Pasternak foundation model, it is given as follows

$$f_e^{Pasternak} = K_w w - K_g \nabla^2 w \tag{15a}$$

K_w is the Winkler parameter, K_g is the shear layer foundation stiffness, and ∇^2 is the Laplace operator in x and y, and w is the plate deflection.

The distributed reaction of the Kerr foundation model is defined as follows: Mekerbi *et al*. (2021)

$$f_e^{kerr} = \left(\frac{k_l k_u}{k_l + k_u}\right) w - \left(\frac{k_s k_u}{k_s + k_u}\right) \nabla^2 w \tag{15b}$$

By replacing the formulation of δU, δV and δU_R in the Eq. (11)

$$\begin{aligned} &\int_V \delta U + \delta V + \delta U_R = \int_A [N_x \delta\varepsilon_x^0 + N_y \delta\varepsilon_y^0 + N_z \delta\varepsilon_z^0 + N_{xy} \delta\gamma_{xy}^0 + M_x^b \delta k_x^b \\ &+ M_y^b \delta k_y^b + M_{xy}^b \delta k_{xy}^b + M_x^s \delta k_x^s + M_y^s \delta k_y^s + M_{xy}^s \delta k_{xy}^s + Q_{yz}^S \delta\gamma_{yz}^0 + S_{yz}^S \delta\gamma_{yz}^1 \\ &+ Q_{xz}^S \delta\gamma_{xz}^0 + S_{xz}^S \delta\gamma_{xz}^1] dA - \int_A q g(z) \delta\phi_z dA + \int_A R \delta w_0 dA + \int_A R g(z) \delta\phi_z dA = 0 \end{aligned} \tag{16}$$

The five equations of equilibrium state in the current case are reached by integration by parts and collecting the unknowns' displacement δu_0, δv_0, δw_0, $\delta\theta$ *and* $\delta\phi_z$

$$\delta u_0: \quad \frac{\partial N_x}{\partial x} + \frac{\partial N_{xy}}{\partial y} = 0 \tag{17a}$$

$$\delta v_0: \quad \frac{\partial N_{xy}}{\partial x}+\frac{\partial N_y}{\partial y}=0 \tag{17b}$$

$$\delta w_0: \quad \frac{\partial^2 M_x^b}{\partial x^2}+2\frac{\partial^2 M_{xy}^b}{\partial x\partial y}+\frac{\partial^2 M_y^b}{\partial y^2}+q-R=0 \tag{17c}$$

$$\delta\theta: \quad -k_1M_x^s-k_2M_y^s-(k_1A'+k_2B')\frac{\partial^2 M_{xy}^s}{\partial x\partial y}+\frac{\partial S_{xz}^s}{\partial x}+\frac{\partial S_{yz}^s}{\partial y}=0 \tag{17d}$$

$$\delta\varphi_z: \quad \frac{\partial S_{xz}^s}{\partial x}+\frac{\partial S_{yz}^s}{\partial y}-N_z+g(z)(q-R)=0 \tag{17e}$$

The in-plane force resultants N, moment resultants M, and the transverse shear stress resultants Q and S are achieved as

$$\begin{Bmatrix} N \\ M^b \\ M^s \end{Bmatrix}=\begin{bmatrix} A & B & B^s \\ B & D & D^s \\ B^s & D^s & H^s \end{bmatrix}\begin{Bmatrix} \varepsilon \\ k^b \\ k^s \end{Bmatrix}+\begin{bmatrix} L \\ L^a \\ R \end{bmatrix}\varepsilon, \quad S=A^s\ \gamma$$
$$N_z=R^a\varepsilon_z^0+L(\varepsilon_x^0+\varepsilon_y^0)+L^a(k_x^b+k_y^b)+R(k_x^s+k_y^s) \tag{18}$$

where

$$A=\begin{bmatrix} A_{11} & A_{12} & 0 \\ A_{12} & A_{22} & 0 \\ 0 & 0 & A_{66} \end{bmatrix},\ B=\begin{bmatrix} B_{11} & B_{12} & 0 \\ B_{12} & B_{22} & 0 \\ 0 & 0 & B_{66} \end{bmatrix},\ D=\begin{bmatrix} D_{11} & D_{12} & 0 \\ D_{12} & D_{22} & 0 \\ 0 & 0 & D_{66} \end{bmatrix},$$
$$B^s=\begin{bmatrix} B_{11}^s & B_{12}^s & 0 \\ B_{12}^s & B_{22}^s & 0 \\ 0 & 0 & B_{66}^s \end{bmatrix},\ D^s=\begin{bmatrix} D_{11}^s & D_{12}^s & 0 \\ D_{12}^s & D_{22}^s & 0 \\ 0 & 0 & D_{66}^s \end{bmatrix},\ \mathrm{H}^s=\begin{bmatrix} H_{11}^s & H_{12}^s & 0 \\ H_{12}^s & H_{22}^s & 0 \\ 0 & 0 & H_{66}^s \end{bmatrix} \tag{19a}$$

$$\begin{Bmatrix} A_{11} & B_{11} & D_{11} & B_{11}^s & D_{11}^s & H_{11}^s \\ A_{12} & B_{12} & D_{12} & B_{12}^s & D_{12}^s & H_{12}^s \\ A_{66} & B_{66} & D_{66} & B_{66}^s & D_{66}^s & H_{66}^s \end{Bmatrix}=\int_{-h/2}^{h/2}\lambda(z)\begin{Bmatrix} 1 \\ z \\ z^2 \\ f(z) \\ zf(z) \\ f^2(z) \end{Bmatrix}^T\begin{Bmatrix} \frac{1-\nu}{\nu} \\ 1 \\ \frac{1-2\nu}{2\nu} \end{Bmatrix}dz \tag{19b}$$

$$\begin{Bmatrix} L \\ L^a \\ R \end{Bmatrix}=\int_{-h/2}^{h/2}C_{ij}\begin{Bmatrix} 1 \\ z \\ f(z) \end{Bmatrix}g'(z)\,dz, if\ (i=1,2\ ;\ j=3)$$
$$\{R^a\}=\int_{-h/2}^{h/2}C_{33}\ [g'(z)]^2dz \tag{19c}$$

$$A^s=\begin{bmatrix} A_{44}^s & 0 \\ 0 & A_{55}^s \end{bmatrix}, \qquad A_{44}^s=A_{55}^s=\int_{-h/2}^{h/2}\left(\frac{E(z)}{2(1+\nu)}\ [g^2(z)]\right)\,dz \tag{19d}$$

$$(A_{22}, B_{22}, D_{22}, B_{22}^s, D_{22}^s, H_{22}^s) = (A_{11}, B_{11}, D_{11}, B_{11}^s, D_{11}^s, H_{11}^s) \tag{19e}$$

By replacing Eq. (18) into Eq. (17), the equation of equilibrium can be rewritten according to displacement terms $(u_0, v_0, w_0, \theta \text{ and } \phi)$ and the form of the equation becomes

$$\begin{aligned}\delta u_0 :\ & A_{11}\frac{\partial^2 u_0}{\partial x^2} + A_{12}\frac{\partial^2 v_0}{\partial x \partial y} + A_{66}\left(\frac{\partial^2 u_0}{\partial y^2} + \frac{\partial^2 v_0}{\partial x \partial y}\right) - B_{11}\frac{\partial^3 w_0}{\partial x^3} - B_{12}\frac{\partial^3 w_0}{\partial x \partial y^2} \\ & -2B_{66}\frac{\partial^3 w_0}{\partial x \partial y^2} + B_{11}^s k_1 \frac{\partial \theta}{\partial x} + B_{12}^s k_2 \frac{\partial \theta}{\partial x} + B_{66}^s (A'k_1 + B'k_2)\frac{\partial^3 \theta}{\partial x \partial y^2} + L\frac{\partial \varphi_z}{\partial x} = 0\end{aligned} \tag{20a}$$

$$\begin{aligned}\delta v_0 :\ & A_{12}\frac{\partial^2 u_0}{\partial x \partial y} + A_{22}\frac{\partial^2 v_0}{\partial y^2} + A_{66}\left(\frac{\partial^2 u_0}{\partial x \partial y} + \frac{\partial^2 v_0}{\partial x^2}\right) - B_{12}\frac{\partial^3 w_0}{\partial x^2 \partial y} - B_{22}\frac{\partial^3 w_0}{\partial y^3} \\ & -2B_{66}\frac{\partial^3 w_0}{\partial x^2 \partial y} + B_{12}^s k_1 \frac{\partial \theta}{\partial y} + B_{22}^s k_2 \frac{\partial \theta}{\partial y} + B_{66}^s (A'k_1 + B'k_2)\frac{\partial^3 \theta}{\partial x^2 \partial y} + L\frac{\partial \varphi_z}{\partial y} = 0\end{aligned} \tag{20b}$$

$$\begin{aligned}\delta w_0 :\ & B_{11}\frac{\partial^3 u_0}{\partial x^3} + B_{12}\left(\frac{\partial^3 u_0}{\partial x \partial y^2} + \frac{\partial^3 v_0}{\partial x^2 \partial y}\right) + B_{22}\frac{\partial^3 v_0}{\partial y^3} + 2B_{66}\left(\frac{\partial^3 u_0}{\partial x \partial y^2} + \frac{\partial^3 v_0}{\partial x^2 \partial y}\right) \\ & -D_{11}\frac{\partial^4 w_0}{\partial x^4} - 2D_{12}\frac{\partial^4 w_0}{\partial x^2 \partial y^2} - D_{22}\frac{\partial^4 w_0}{\partial y^4} - 4D_{66}\frac{\partial^4 w_0}{\partial x^2 \partial y^2} + D_{11}^s k_1 \frac{\partial^2 \theta}{\partial x^2} \\ & +D_{12}^s\left(k_1\frac{\partial^2 \theta}{\partial y^2} + k_2\frac{\partial^2 \theta}{\partial x^2}\right) + D_{22}^s k_2 \frac{\partial^2 \theta}{\partial y^2} + 2D_{66}^s (A'k_1 + B'k_2)\theta\frac{\partial^4 \theta}{\partial x^2 \partial y^2} \\ & +L^a\left(\frac{\partial^2 \varphi_z}{\partial x^2} + \frac{\partial^2 \varphi_z}{\partial y^2}\right) + q - R = 0\end{aligned} \tag{20c}$$

$$\begin{aligned}\delta\theta :\ & -B_{11}^s k_1 \frac{\partial u_0}{\partial x} - B_{12}^s\left(k_1\frac{\partial v_0}{\partial y} + k_2\frac{\partial u_0}{\partial x}\right) - B_{22}^s k_2 \frac{\partial v_0}{\partial y} \\ & -B_{66}^s (A'k_1 + B'k_2)\left(\frac{\partial^3 u_0}{\partial x \partial y^2} + \frac{\partial^3 v_0}{\partial x^2 \partial y}\right) + D_{11}^s k_1 \frac{\partial^2 w_0}{\partial x^2} + D_{12}^s\left(k_1\frac{\partial^2 w_0}{\partial y^2} + k_2\frac{\partial^2 w_0}{\partial x^2}\right) \\ & +D_{22}^s k_2 \frac{\partial^2 w_0}{\partial y^2} + 2D_{66}^s (A'k_1 + B'k_2)\frac{\partial^4 w_0}{\partial x^2 \partial y^2} - H_{11}^s (k_1)^2\theta - 2H_{12}^s k_1 k_2 \theta \\ & -H_{22}^s (k_2)^2\theta - H_{66}^s (A'k_1 + B'k_2)^2\frac{\partial^4 \theta}{\partial x^2 \partial y^2} + A_{55}^s (A'k_1)\frac{\partial^2 \theta}{\partial x^2} \\ & +A_{44}^s (B'k_2)\frac{\partial^2 \theta}{\partial y^2} + R(k_1 + k_2)\varphi_z + A_{55}^s A'k_1 \frac{\partial^2 \varphi_z}{\partial x^2} + A_{44}^s B'k_2 \frac{\partial^2 \varphi_z}{\partial y^2} = 0\end{aligned} \tag{20d}$$

$$\begin{aligned}\delta\varphi_z :\ & -L\left(\frac{\partial u_0}{\partial x} + \frac{\partial v_0}{\partial y}\right) + L^a\left(\frac{\partial^2 w_0}{\partial x^2} + \frac{\partial^2 w_0}{\partial y^2}\right) + \left(k_2(A_{44}^s - R) + k_1(A_{55}^s - R)\right)\theta \\ & -R^a\varphi_z + A_{55}^s\frac{\partial^2 \varphi_z}{\partial x^2} + A_{44}^s\frac{\partial^2 \varphi_z}{\partial y^2} = 0\end{aligned} \tag{20e}$$

Support types are typically used to evaluate FG plates. This study examines the exact solutions of Eqs. (20 (a)-(e)). In this particular problem, where the FG plate is considered to be simply supported at the plate boundaries, the following settings are imposed.

$$\begin{aligned} v_0 = w_0 = \theta = \theta_{,y} = \varphi = N_x = M_x^b = M_x^s = 0 \quad \text{at } x{=}0, a \\ u_0 = w_0 = \theta = \theta_{,x} = \varphi = N_y = M_y^b = M_y^s = 0 \quad \text{at } y{=}0, b \end{aligned} \tag{21}$$

Following the Navier process for resolving this problem, the following solutions are adapted for $u_0, v_0, w_0, \theta \; and \; \phi_z$, that satisfies the boundary conditions given as

$$\begin{Bmatrix} u_0 \\ v_0 \\ w_0 \\ \theta \\ \varphi_z \end{Bmatrix} = \begin{Bmatrix} U_{mn} \, cos(\alpha \, x) \, sin(\beta \, y) \\ V_{mn} \, sin(\alpha \, x) \, cos(\beta \, y) \\ W_{mn} \, sin(\alpha \, x) \, sin(\beta \, y) \\ X_{mn} \, sin(\alpha \, x) \, sin(\beta \, y) \\ \Phi_{mn} \, sin(\alpha \, x) \, sin(\beta \, y) \end{Bmatrix} \tag{22}$$

where U_{mn}, V_{mn}, W_{mn}, X_{mn} and Φ_{mn} are arbitrary parameters for determination.

Transverse mechanical loads q is assumed as a double Fourier series shape and expressed by:

$$\begin{aligned} q(x,y) &= \sum_{m=1,3,5}^{\infty} \sum_{n=1,3,5}^{\infty} q_{mn} \, sin(\alpha \, x) \, sin(\beta \, y) \\ q_{mn} &= \frac{4}{ab} \int_0^b \int_0^a q(x,y) \; sin(\alpha \, x) \, sin(\beta \, y) dx dy \end{aligned} \tag{23}$$

The values of q_{mn} using Eq. (23) are set as follows

$$\text{For SDL} \Rightarrow \boldsymbol{q_{mn} = q_0} \quad \boldsymbol{if} \; (\boldsymbol{m = n = 1}) \tag{24a}$$

$$\text{For UDL} \Rightarrow q_{mn} = \begin{cases} \dfrac{16 \, q_0}{m \, n \, \pi^2} & m, n = 1, 3, 5 \; \ldots \\ 0 & m, n = 2, 4, 6 \; \ldots \end{cases} \tag{24b}$$

$$\begin{aligned} \text{For CCL} \Rightarrow q_{mn} &= \frac{4 \, p_0}{a \, b} \, sin\left(\frac{m \, \pi \, x}{a}\right) \, sin\left(\frac{n \, \pi \, y}{b}\right) \\ \text{Avec } m &= 25, n = 25, p_0 = q_0 \, (a \, b) \end{aligned} \tag{24c}$$

$$\begin{aligned} \text{For PDL} \Rightarrow q_{mn} &= \begin{cases} \dfrac{16 \, q_0}{m \, n \, \pi^2} X_m Y_n & m, n = 1, 3, 5 \; \ldots \\ 0 & m, n = 2, 4, 6 \; \ldots \end{cases} \\ X_m &= \left[\sin\left(\frac{m \, \pi}{a} \, x_0 \right) \right] \left[\sin\left(\frac{m \, \pi}{2 \, a} \, a_0 \right) \right] \\ Y_n &= \left[\sin\left(\frac{n \, \pi}{b} \, y_0 \right) \right] \left[\sin\left(\frac{n \, \pi}{2 \, b} \, b_0 \right) \right] \end{aligned} \tag{24d}$$

The substitution of Eq. (22) and Eq. (23) into Eqs. (20 (a)-(e)) shows that the analytical solutions of the present case may be established through

$$\left[a_{ij}\right]\{\delta\} = \{F\} \;\; \text{with} \;\; i, j = 1,2,3,4 \; \& \; 5. \tag{25}$$

In which

Table 1 FG plate material characteristics

Proprieties	Mechanical case	
	Aluminum	Alumina
E	70	380
υ	0.3	0.3

$$\{F\} = \begin{Bmatrix} F_1 = 0 \\ F_2 = 0 \\ F_3 = -qmn \\ F_4 = 0 \\ F_5 = 0 \end{Bmatrix} \text{ and } \{\delta\} = \begin{Bmatrix} U_{mn} \\ V_{mn} \\ W_{mn} \\ X_{mn} \\ \Phi_{mn} \end{Bmatrix} \tag{26}$$

and

$$\begin{aligned}
a_{11} &= -A_{11}\alpha^2 - A_{66}\beta^2 \\
a_{12} &= -(A_{66} + A_{12})\alpha\beta \\
a_{13} &= B_{11}\alpha^3 - (-B_{12} - 2B_{66})\alpha\beta^2 \\
a_{14} &= -BS_{66}(Ak_1 + Bk_2)\alpha\beta^2 + (BS_{11}k_1 + BS_{12}k_2)\alpha \\
a_{15} &= A_{13}\alpha \\
a_{22} &= -A_{22}\beta^2 - A_{66}\alpha^2 \\
a_{23} &= B_{22}\beta^3 + (B_{12} + 2B_{66})\alpha^2\beta \\
a_{24} &= -BS_{66}(Ak_1 + Bk_2)\alpha^2\beta + (BS_{12}k_1 + BS_{11}k_2)\beta \\
a_{25} &= A_{23}\beta \\
a_{33} &= -D_{11}\alpha^4 - 2(D_{12} + 2D_{66})\alpha^2\beta^2 - D_{22}\beta^4 - K_w - K_p(\alpha^2 + \beta^2) \\
a_{34} &= -(DS_{11}k_1 + DS_{12}k_2)\alpha^2 - (DS_{12}k_1 + DS_{22}k_2)\beta^2 + 2DS_{66}(Ak_1 + Bk_2)\alpha^2\beta^2 \\
a_{35} &= -B_{13}\alpha^2 - B_{23}\beta^2 \\
a_{44} &= -(k_1A)^2AS_{55}\alpha^2 - (k_2B)^2AS_{44}\beta^2 - HS_{66}(Ak_1 + Bk_2)^2\alpha^2\beta^2 \\
&\quad -k_1(HS_{11}k_1 + HS_{12}k_2) - k_2(HS_{12}k_1 + HS_{22}k_2) \\
a_{45} &= -Ak_1AS_{55}\alpha^2 - k_2BAS_{44}\beta^2 - BS_{13}k_1 - BS_{23}k_2 \\
a_{55} &= -AS_{55}\alpha^2 - AS_{44}\beta^2 - A_{33}
\end{aligned} \tag{27}$$

3. Numerical results and discussion

This section is dedicated to discussing the outcomes from analyzing the thermo-hygro-mechanical bending behavior of the FG plate, taking into account two elastic foundation parameters. It will be divided into three distinct parts: the first will focus on result validation, the second will involve a parametric study, and the final part will examine the effects of different power laws on the behavior of FG plates on uniform and variable foundations. The FG plate is composed of titanium alloy (Ti-6Al-4V) and zirconia (ZrO2). The mechanical properties of the plate, including Young's modulus E, Poisson's ratio are presented in Table 1.

The numerical results of this investigation are presented regarding non-dimensional deflection and stresses. The calculation formulas of the dimensionless terms are:

Table 2 Nondimensionalized deflection $\bar{w}(0)$ of and the in-plane normal stress $\bar{\sigma}_{xx}(h/3)$in FG square plates under sinusoidal loads

k	Theory	$\overline{w}$			$\overline{\sigma}_{xx}$		
		a/h			a/h		
		4	10	100	4	10	100
1	Zenkour *et al*. [24]	0.6896	0.5680	0.5446	0.5706	1.4159	14.1343
	Present Quasi-3D	0.6913	0.5694	0.5460	0.5807	1. 4489	14. 4789
4	Zenkour *et al*. [24]	1.0970	0.8403	0.7910	0.4181	1.0802	10.8630
	Present Quasi-3D	1.0987	0.8422	0.7930	0.4311	1.1206	11.2818
10	Zenkour *et al*. [24]	1.3333	0.9807	0.9130	0.3033	0.8031	8.1112
	Present Quasi-3D	1.3357	0.9820	0.9142	0.3151	0.8392	8.4849

$$\begin{aligned}
&\overline{w} = \frac{10^2 D}{q_0 a^4} w\left(\frac{a}{2},\frac{b}{2},\frac{z}{h}\right), \quad w* = \frac{10h^3 E_c}{q_0 a^4} w\left(\frac{a}{2},\frac{b}{2},\frac{z}{h}\right), \quad w** = \frac{100h}{q_0 a^2} w\left(\frac{a}{2},\frac{b}{2},\frac{z}{h}\right),\\
&\sigma_1 = \frac{h}{q_0 a}\sigma_{xx}\left(\frac{a}{2},\frac{b}{2},\frac{z}{h}\right), \quad \sigma_3 = \frac{h}{q_0 a}\sigma_{zz}\left(\frac{a}{2},\frac{b}{2},\frac{z}{h}\right), \quad \sigma_4 = \frac{10}{q_0}\sigma_{yx}\left(\frac{a}{2},0,\frac{z}{h}\right),\\
&\sigma_5 = \frac{10h}{q_0 a}\sigma_{xz}\left(0,\frac{b}{2},\frac{z}{h}\right), \quad \sigma_6 = \frac{h}{q_0 a}\sigma_{xy}\left(0,0,\frac{z}{h}\right),\\
&k_w = \frac{a^4}{D}K_w, \quad k_p = \frac{a^2}{D}K_p, \quad D = \frac{h^3 Ec}{12(1-\nu^2)}
\end{aligned} \tag{28}$$

The numerical results of this investigation are presented regarding non-dimensional deflection and stresses. The calculation formulas of the dimensionless terms are:

3.1 Comparative study

Table 2 provides a comparative analysis of nondimensionalized deflection ($\bar{w}$) and in-plane normal stress ($\bar{\sigma}_{xx}$) for functionally graded square plates subjected to sinusoidal loading. The results obtained from the current theoretical framework demonstrate strong agreement with Zenkour *et al*. (2014) for Quasi-3D theory ($\varepsilon_z \neq 0$). It is noteworthy that the deflection ($\bar{w}$) exhibits a decreasing trend with increasing side-to-thickness ratio (*a/h*) and decreasing volume fraction index (*k*), while the in-plane normal stress ($\bar{\sigma}_{xx}$) increases correspondingly.

Table 3 presents a comparative analysis of non-dimensionalized deflection for homogeneous plates resting on a Winkler-Pasternak foundation under uniformly distributed loads. The influence of various side-to-thickness ratios (*a/h*) and foundation parameters (*Kw*, *Kp*) is investigated. The results obtained from the current theoretical framework are compared with Zenkour *et al*. (2014) for quasi-3D theory. It is observed that the plate deflection decreases with increasing foundation parameters and side-to-thickness ratios. For all (*a/h*) values, the current method strongly agrees with the reference results in Table 3.

Table 4 presents a comparative analysis of non-dimensional stresses and deflection for isotropic homogeneous and functionally graded square plates with varying volume fraction indices. The results are compared with those of Zenkour *et al*. (2014) based on transverse shear and normal deformation plate theory. It is observed that shear stress, axial stress, and deflection decrease with increasing foundation parameters (*kw*, *kp*). The volume fraction index (*k*) significantly influences

Table 3 Comparisons of central deflections $10\,\bar{w}$ of a uniformly loaded homogeneous square plate resting on elastic foundations (m, n = 100 term series)

Theory	a/h	kw= 1 kp			
		5	10	15	20
Zenkour *et al*. (2014)	5	3.669	2.976	2.500	2.154
Present Quasi-3D		3.6768	2.9801	2.5031	2.1565
		kw = 3^4			
Zenkour *et al*. (2014)		3.078	2.571	2.206	1.931
Present Quasi-3D		3.0826	2.5742	2.2083	1.9327
		$kw = 5^4$			
Zenkour *et al*. (2014)		1.431	1.308	1.204	1.115
Present Quasi-3D		1.4319	1.3084	1.2045	1.1159
	a/h	kw= 1 kp			
		5	10	15	20
Zenkour *et al*. (2014)	10	3.330	2.745	2.333	2.027
Present Quasi-3D		3.3373	2.7499	2.3363	2.0295
		kw = 3^4			
Zenkour *et al*. (2014)		2.836	2.398	2.075	1.829
Present Quasi-3D		2.8409	2.4013	2.0781	1.8306
		$kw = 5^4$			
Zenkour *et al*. (2014)		1.385	1.268	1.169	1.085
Present Quasi-3D		1.3865	1.2692	1.1701	1.0853
	a/h	kw= 1 kp			
		5	10	15	20
Zenkour *et al*. (2014)	20	3.212	2.663	2.272	1.980
Present Quasi-3D		3.2190	2.6677	2.2757	1.9830
		kw = 3^4			
Zenkour *et al*. (2014)		2.749	2.335	2.027	1.791
Present Quasi-3D		2.7545	2.3384	2.0302	1.7929
		$kw = 5^4$			
Zenkour *et al*. (2014)		1.367	1.253	1.156	1.073
Present Quasi-3D		1.3686	1.2541	1.1571	1.0739

the stress and deflection behaviour of both isotropic homogeneous and functionally graded plates. The deflection increases with increasing volume fraction index (k) due to the reduction in bending stiffness, which is maximum for a fully ceramic plate ($k = 0$). In the absence of elastic foundations, the stresses in fully ceramic and fully metallic plates are identical, demonstrating that the stresses

Table 4 Nondimensionalized deflection $\bar{w}(0)$ of and stresses σi in FG square plates resting on elastic foundations under sinusoidal loads (a = 10h)

$(\bar{w}, \sigma_i)$	(kw,kp)	Theory	k					
			Ceramic	1	2	5	10	Metal
$\bar{w}$	(0,0)	Zenkour *et al*. (2014)	0.29334	0.56802	0.71988	0.87256	0.98072	1.59239
		Present Quasi-3D	0.29415	0.56939	0.72195	0.87418	0.98200	1.59679
	(100,0)	Zenkour *et al*. (2014)	0.23171	0.37476	0.43524	0.48679	0.51890	0.65161
		Present Quasi-3D	0.23221	0.37534	0.43597	0.48724	0.51916	0.65229
	(0,10)	Zenkour *et al*. (2014)	0.19235	0.28149	0.31424	0.34028	0.35575	0.41361
		Present Quasi-3D	0.19269	0.28181	0.31460	0.34047	0.35583	0.41387
	(100,10)	Zenkour *et al*. (2014)	0.16379	0.22419	0.24445	0.25994	0.26893	0.30081
		Present Quasi-3D	0.16403	0.22440	0.24467	0.26004	0.26895	0.30093
$\bar{\sigma}_{xx}$ (h /2)	(0,0)	Zenkour *et al*. (2014)	2.12463	3.27707	3.82256	4.47146	5.32910	2.12463
		Present Quasi-3D	2.03137	3.11958	3.64669	4.27100	5.10271	2.03137
	(100,0)	Zenkour *et al*. (2014)	1.67827	2.16212	2.31114	2.49458	2.81963	0.86939
		Present Quasi-3D	1.60362	2.05643	2.20219	2.38051	2.69770	0.82981
	(0,10)	Zenkour *et al*. (2014)	1.39321	1.62400	1.66859	1.74376	1.93308	0.55186
		Present Quasi-3D	1.33073	1.54397	1.58910	1.66343	1.84898	0.52651
	(100,10)	Zenkour *et al*. (2014)	1.18631	1.29346	1.29805	1.33209	1.46131	0.40135
		Present Quasi-3D	1.13279	1.22941	1.23585	1.27047	1.39753	0.38283
$\bar{\sigma}_{xy}$ (-h /3)	(0,0)	Zenkour *et al*. (2014)	0.69856	0.56467	0.49269	0.52346	0.54777	0.69856
		Present Quasi-3D	0.70068	0.56582	0.49413	0.52449	0.54795	0.70068
	(100,0)	Zenkour *et al*. (2014)	0.55179	0.37256	0.29789	0.29203	0.28983	0.28585
		Present Quasi-3D	0.55314	0.37299	0.29839	0.29233	0.28969	0.28623
	(0,10)	Zenkour *et al*. (2014)	0.45807	0.27983	0.21507	0.20414	0.19869	0.18145
		Present Quasi-3D	0.45901	0.28005	0.21532	0.20427	0.19855	0.18161
	(100,10)	Zenkour *et al*. (2014)	0.39005	0.22288	0.16731	0.15594	0.15021	0.13196
		Present Quasi-3D	0.39073	0.22299	0.16746	0.15602	0.15007	0.13205
$\bar{\sigma}_{xz}$ (0)	(0,0)	Zenkour *et al*. (2014)	0.24541	0.24541	0.22581	0.20107	0.21916	0.24541
		Present Quasi-3D	0.24168	0.24168	0.22178	0.19642	0.21472	0.24168
	(100,0)	Zenkour *et al*. (2014)	0.19385	0.16191	0.13652	0.11217	0.11596	0.10042
		Present Quasi-3D	0.19079	0.15932	0.13393	0.10948	0.11352	0.09873
	(0,10)	Zenkour *et al*. (2014)	0.16093	0.12162	0.09857	0.07841	0.07949	0.06374
		Present Quasi-3D	0.15832	0.11961	0.09665	0.07650	0.07780	0.06264
	(100,10)	Zenkour *et al*. (2014)	0.13703	0.09686	0.07668	0.05990	0.06009	0.04636
		Present Quasi-3D	0.13477	0.09524	0.07516	0.05843	0.05881	0.04555

are independent of the modulus of elasticity for homogeneous materials. The excellent agreement between the present results and those reported in Table 4 validates the effectiveness of the current methods.

Table 5 Non-dimensional deflection $\overline{w}$ and normal stress $\overline{\sigma}_{xx}$ and transverse shear stress $\overline{\sigma}_{xz}$ of FGM square plates under uniform loads without Winkler–Pasternak foundations

(Kw, Kp)	k	$\overline{w}\left(\frac{a}{2},\frac{b}{2},0\right)$			$\overline{\sigma}_{xx}\left(\frac{a}{2},\frac{b}{2},\frac{h}{2}\right)$			$\overline{\sigma}_{xz}\left(0,\frac{b}{2},0\right)$		
		a/h								
		5	10	20	5	10	20	5	10	20
(0, 0)	0	0.52445	0.46380	0.44853	1.51452	2.94041	5.83643	0.48433	0.49871	0.50591
	1	1.00068	0.89823	0.87244	2.33160	4.51347	8.95208	0.48433	0.49872	0.50591
	2	1.28306	1.13847	1.10208	2.73395	5.27327	10.44889	0.44382	0.45737	0.46414
	5	1.61690	1.37660	1.31614	3.22499	6.16787	12.19510	0.39209	0.40463	0.41091
	10	1.84243	1.54561	1.47092	3.84726	7.37103	14.58042	0.42856	0.44232	0.44919
	∞	2.84700	2.51779	2.43487	1.51451	2.94040	5.83639	0.48433	0.49871	0.50591
(100, 0)	0	0.39982	0.36357	0.35404	1.12405	2.25227	4.50491	0.39337	0.41555	0.42468
	1	0.62549	0.58430	0.57323	1.38171	2.80542	5.62940	0.34033	0.36394	0.37344
	2	0.72212	0.67592	0.66327	1.43617	2.95460	5.94880	0.28962	0.31346	0.32288
	5	0.81053	0.75103	0.73407	1.48270	3.13792	6.36472	0.23628	0.26200	0.27183
	10	0.86086	0.79751	0.77906	1.63441	3.51923	7.17106	0.24639	0.27615	0.28741
	∞	1.03210	0.99157	0.97967	0.47520	1.01962	2.07512	0.23698	0.26349	0.27382
(0, 10)	0	0.32607	0.30084	0.29409	0.91270	1.84756	3.70629	0.32530	0.35558	0.36697
	1	0.46135	0.43699	0.43038	1.01655	2.07379	4.16912	0.25482	0.28697	0.29913
	2	0.51146	0.48589	0.47889	1.02062	2.10149	4.23575	0.20668	0.23873	0.25106
	5	0.55466	0.52325	0.51444	1.03211	2.17171	4.40429	0.15898	0.19277	0.20618
	10	0.57857	0.54538	0.53599	1.12610	2.39756	4.87786	0.16020	0.19897	0.21468
	∞	0.65296	0.62967	0.62328	0.314356	0.654302	1.32237	0.14073	0.17700	0.19224
(100, 10)	0	0.27223	0.25451	0.24968	0.74494	1.53085	3.08279	0.28561	0.31686	0.32854
	1	0.35896	0.34433	0.34029	0.76001	1.57385	3.17659	0.21480	0.24662	0.25872
	2	0.38727	0.37313	0.36923	0.73705	1.54232	3.12233	0.17177	0.20299	0.21516
	5	0.40971	0.39374	0.38930	0.72361	1.55261	3.16587	0.13023	0.16255	0.17567
	10	0.42196	0.40560	0.40105	0.77848	1.68818	3.45204	0.13030	0.16710	0.18239
	∞	0.45982	0.44838	0.44540	0.20610	0.43113	0.87242	0.11336	0.14794	0.16279

3.2 Parametric study

3.2.1 Numerical results

This study investigates the bending behavior of functionally graded plates under sinusoidal and uniform loads. It analyses the influence of various parameters, including foundation type, power-law index, plate geometry, and stress and displacement distribution through the thickness under various partial loads.

Tables 5 and 6 present a parametric analysis of non-dimensional stresses and deflections for isotropic homogeneous and functionally graded square plates, considering varying side-to-thickness ratios (a/h). It was observed that shear stress, axial stress, and deflection decreased with increasing Winkler-Pasternak (kw, kp) and Kerr (Ku, Ks) foundation parameters. The volume fraction index

Table 6 Non-dimensional deflection $\overline{w}$ and normal stress $\overline{\sigma}_{xx}$ and transverse shear stress $\overline{\sigma}_{xz}$ of FGM square plates under uniform loads without Kerr foundations, (Kl=100)

(Kw, Kp)	k	$\overline{w}\left(\frac{a}{2},\frac{b}{2},0\right)$			$\overline{\sigma}_{xx}\left(\frac{a}{2},\frac{b}{2},\frac{h}{2}\right)$			$\overline{\sigma}_{xz}\left(0,\frac{b}{2},0\right)$		
		a/h								
		5	10	20	5	10	20	5	10	20
(0, 0)	0	0.52445	0.46380	0.44853	1.51452	2.94041	5.83643	0.48433	0.49871	0.50591
	1	1.00068	0.89823	0.87244	2.33160	4.51347	8.95208	0.48433	0.49872	0.50591
	2	1.28306	1.13847	1.10208	2.73395	5.27327	10.44889	0.44382	0.45737	0.46414
	5	1.61690	1.37660	1.31614	3.22499	6.16787	12.19510	0.39209	0.40463	0.41091
	10	1.84243	1.54561	1.47092	3.84726	7.37103	14.58042	0.42856	0.44232	0.44919
	∞	2.84700	2.51779	2.43487	1.51451	2.94040	5.83639	0.48433	0.49871	0.50591
(100, 0)	0	0.51998	0.46358	0.44852	1.50049	2.93891	5.83624	0.48108	0.49854	0.50590
	1	0.98450	0.89741	0.87240	2.29054	4.50902	8.95151	0.47816	0.49836	0.50591
	2	1.25649	1.13715	1.10200	2.67216	5.26657	10.44826	0.43656	0.45696	0.46413
	5	1.57460	1.37466	1.31603	3.13298	6.15841	12.19398	0.38399	0.40420	0.41088
	10	1.78765	1.54316	1.47078	3.72288	7.35832	14.57884	0.41852	0.44177	0.44915
	∞	2.71990	2.51130	2.43450	1.44105	2.93217	5.83548	0.46729	0.49773	0.50585
(0, 10)	0	0.29583	0.39621	0.43857	0.82243	2.48480	5.58960	0.30001	0.44006	0.49013
	1	0.40252	0.67470	0.80757	0.87761	3.32083	8.24213	0.22772	0.39816	0.47628
	2	0.43969	0.80120	1.00049	0.86760	3.61694	9.42223	0.18232	0.34711	0.43041
	5	0.47076	0.91131	1.17370	0.86701	3.96335	10.7886	0.13824	0.29247	0.37576
	10	0.48782	0.98213	1.29521	0.94033	4.53426	12.7256	0.13826	0.30958	0.40674
	∞	0.53990	1.30127	1.98828	0.25688	1.44442	4.69728	0.11948	0.29970	0.43250
(100, 10)	0	0.09839	0.23818	0.36538	0.25397	1.43440	4.68509	0.11837	0.29828	0.43170
	1	0.10711	0.31517	0.60420	0.21406	1.45112	6.03071	0.07350	0.22636	0.38215
	2	0.10916	0.33927	0.70564	0.19866	1.41920	6.46581	0.05443	0.18421	0.33082
	5	0.11072	0.35650	0.78709	0.19139	1.43041	7.00881	0.03779	0.14558	0.27838
	10	0.11171	0.36640	0.83961	0.20370	1.55701	7.96765	0.03624	0.14847	0.29412
	∞	0.11455	0.40178	1.08235	0.05131	0.40157	2.42609	0.02899	0.12829	0.27804

(k) significantly influenced the stress and deflection behavior of both isotropic homogeneous and functionally graded plates. The deflection increased with increasing side-to-thickness ratios (a/h) due to a combination of reduced stiffness, increased shear deformation, and stress concentration, which was most pronounced in thin plates (a/h=20). In the absence of elastic foundations, the stresses in fully ceramic and fully metallic plates were identical, indicating that stresses are independent of the modulus of elasticity for homogeneous materials.

3.2.2 Graphical illustration

Fig. 2 shows the dimensionless central deflection along the x direction of the plate for different loads, distributed uniformly over (100%, 75%, 25%) of the plate surface and a point load, without foundation and with a Winkler-Pasternak foundation model. It is clear that the highest values of the

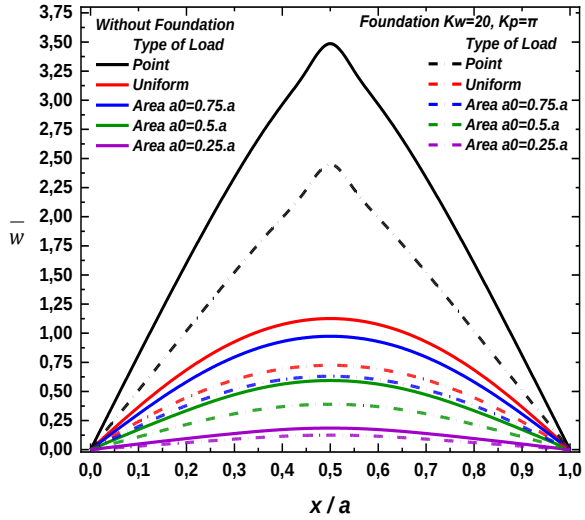

Fig. 2 The dimensionless deflections of square PFG plate under point load, uniform and partially distributed load (3/4, 1/2 and 1/4), where k=2, a/h=10, Kw=20, Kp=π

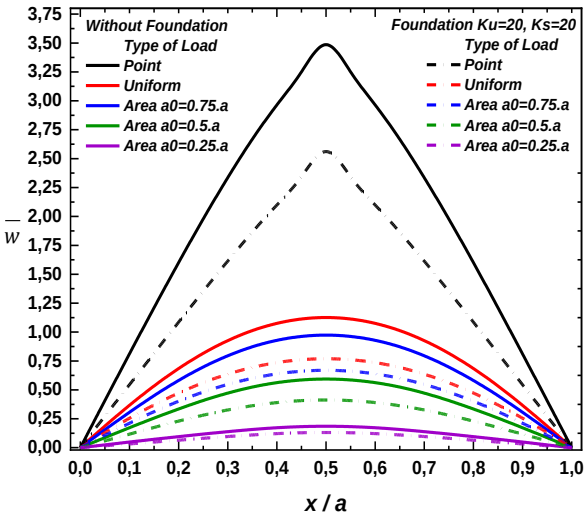

Fig. 3 The dimensionless deflections of square PFG plate under point load, uniform and partially distributed load (3/4, 1/2 and 1/4), where *k=2*, *a/h=10*, *Kl=20*, *Ku=20*, *Ks= 20*

dimensionless central deflection are obtained for the concentrated load. However, the lowest values were obtained for loads distributed uniformly over 25% of the plate surface.

Fig. 3 shows the dimensionless central deflection along the x direction of the plate for different loads, distributed uniformly over (100%, 75%, 25%) of the plate surface and a point load, without foundation and with the Kerr foundation model. It is clear that the highest values of the dimensionless central deflection are obtained for the concentrated load. However, the lowest values were obtained for loads distributed uniformly over 25% of the plate surface.

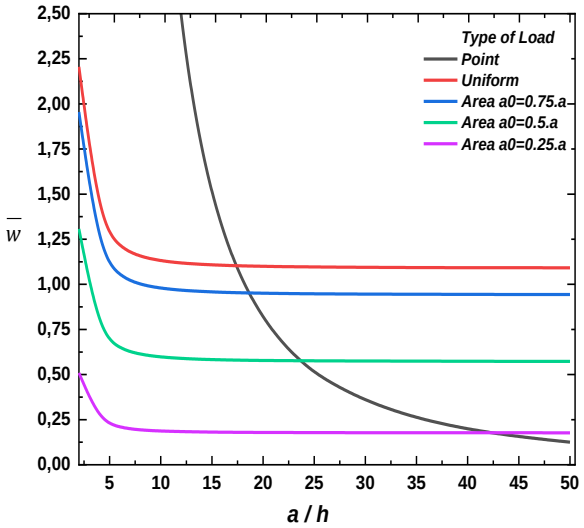

Fig. 4 The non-dimensional central deflections of square PFG plate as a function of side-to-thickness ratio, under *p*oint load, uniform and partially distributed load (3/4, 1/2 and 1/4), *k=2*

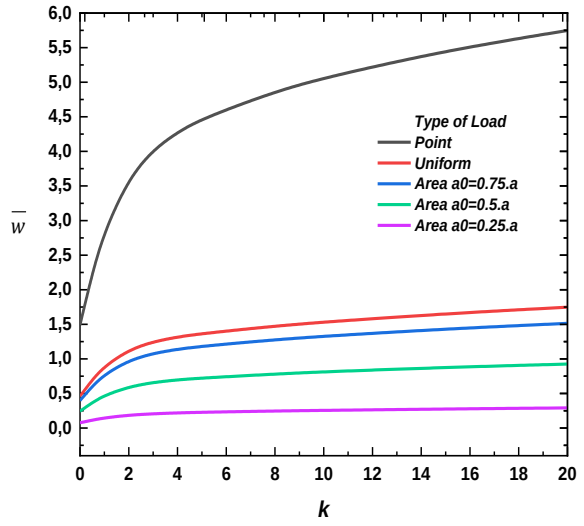

Fig. 5 The non-dimensional central deflections of square PFG plate as a function of side-to-thickness ratio, under *p*oint load, uniform and partially distributed load (3/4, 1/2 and 1/4), *k=2*

Fig. 4 shows the variation of the non-dimensional central deflection concerning the thickness ratio "a/h" subjected to mechanical loads (concentrated load and uniform distributed load 100%, 75%, and 50% of the surface of the plate without foundation). It can be seen that the non-dimensional central deflection decreases when the thickness ratio increases.

Fig. 5 presents the effect of the power law index "k" on the dimensionless central deflection using various mechanical loads. Full ceramic plates show the minimum non-dimensional central deflection. However, increasing the power law index *"k"* leads to an increase in non-dimensional central deflection.

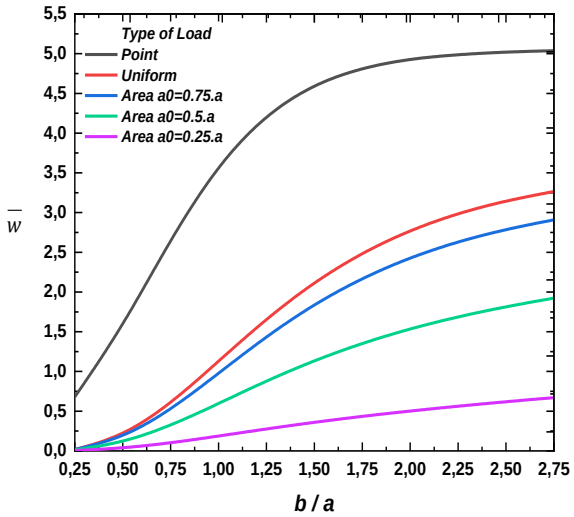

Fig. 6 The deflections of square PFGM plate as a function of aspect ratio "b/a", under point load, uniform and partially distributed load (3/4, 1/2 and 1/4), k=2 and a/h=10

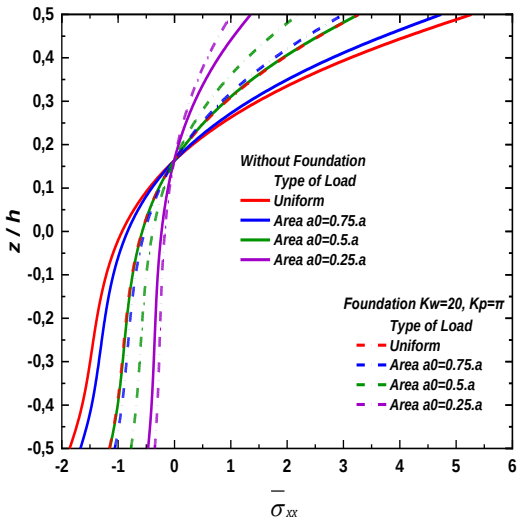

Fig. 7 The non-dimensional axial stresses $\overline{\sigma}_{xx}$ of square P-FGM plate as a function of z-direction under uniform load and partially load (3/4, 1/2 and 1/4) (k=2 and a/h = 10)

Fig. 6 shows the effect of the geometrical ratio "b/a" on the dimensionless central deflection. It can be seen that dimensionless central deflection increases as "b/a" increases. Whatever the type of loading, the deflection follows the same trend as the previous curves.

Figs. 7-8 shows the evolution of the dimensionless axial stress subjected respectively to a uniformly distributed load over (100%, 75%, 25%) of the plate surface and a central concentrated load, without foundation and with the Winkler-Pasternak model. As shown in Fig. 5, the effect of Winkler-Pasternak foundations and without foundation on the dimensionless normal stresses is significant. However, for the central concentrated load, in particular, the normal stresses are tensile at the top surface and compressive at the bottom surface for both loads.

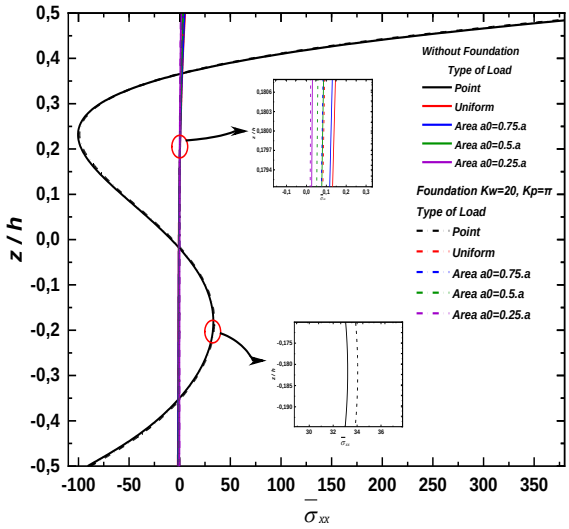

Fig. 8 The non-dimensional axial stresses $\overline{\sigma}_{xx}$ of square P-FGM plate as a function of z-direction under partially load (1/4, 1/2, 3/4 and 1) and point load (k=2 and a/h = 10)

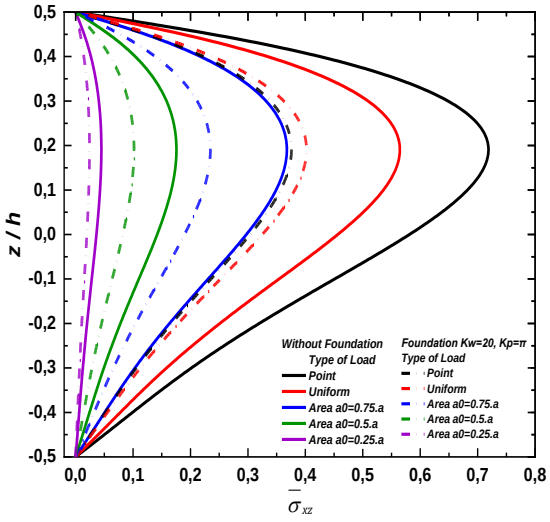

Fig. 9 The shear stresses $\overline{\sigma}_{xz}$ of a P-FGM, the square plate under uniform load, line load, point load, and partially load (3/4, 1/2, and 1/4), where k=2, a/h=10, Kw=20, Kp=π

Fig. 9 shows the variation of the non-dimensional transverse shear stresses for a uniformly distributed load on (100%, 75%, and 25%) of the plate surface and a point load, respectively. For these types of loading, the maximum dimensionless transverse shear stress depends on the type of loading. In addition, the evolution of the non-dimensionless transverse shear stresses is smooth for this type of loading. However, the magnitude of the shear stress is significantly higher for the point load case without any foundation. In contrast, when an elastic support is present, the shear stress values for the point load become closer to those observed under uniform distribution loading.

Fig. 10 shows the dimensionless central deflection along the x-direction of the plate for a

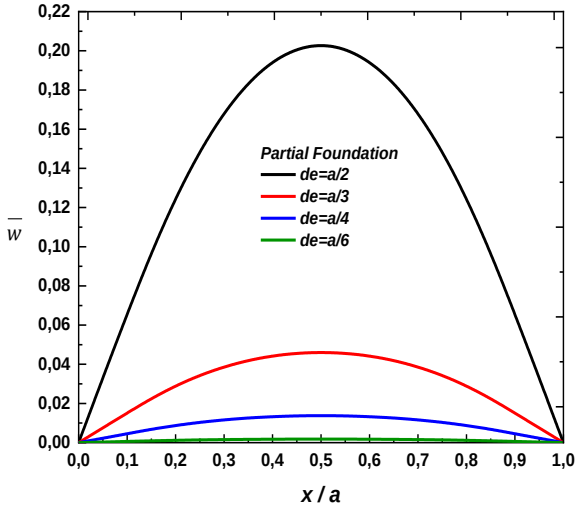

Fig. 10 The dimensionless central deflection of square P-FGM plate under uniform load with a variable-sized Kerr foundation "***de***" (k=2, a/h=10, Kl=20, Ku=20, Ks=20)

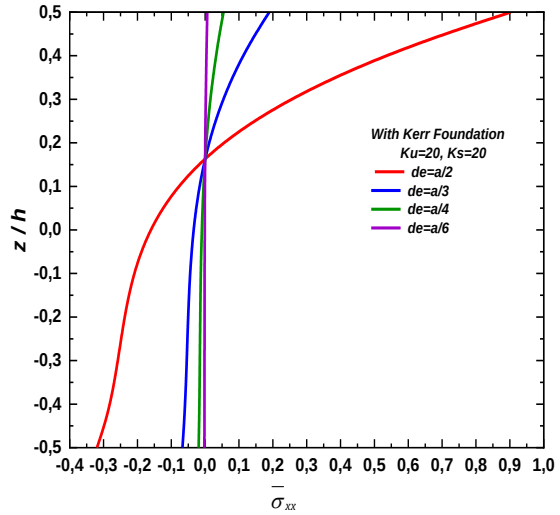

Fig. 11 The nondimensional axial stresses $\overline{\sigma}_{xx}$ of square P-FGM plate under uniform load and with a variable-sized Kerr foundation "***de***" (k=2, a/h=10, Kl=20, Ku=20, Ks=20).

uniformly distributed load and with a variable-sized Kerr foundation. Moreover, the highest values of the dimensionless central deflection are obtained for the widest foundations.

Fig. 11 shows the dimensionless axial stress through the plate thickness for a uniformly distributed load and with a variable-sized Kerr foundation "de", Moreover, the highest values of the dimensionless normal stress are obtained for the widest foundations.

Fig. 12 shows the dimensionless transverse shear stress for a uniformly distributed load and with a variable-sized Kerr foundation "*de*", However, the highest values of the dimensionless transverse shear stress are obtained for the widest foundations.

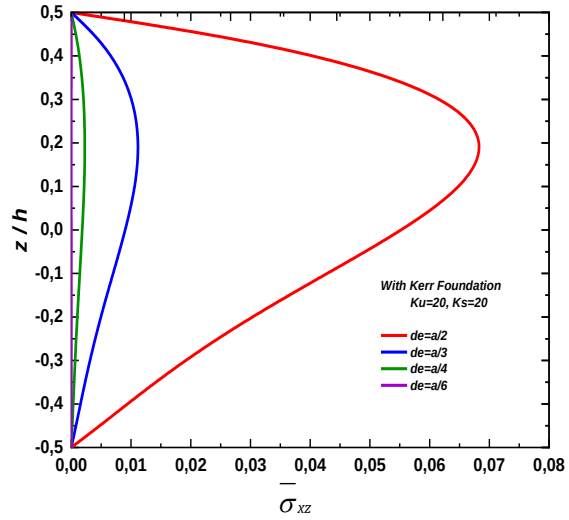

Fig. 12 The nondimensional shear stresses$\overline{\sigma}_{xz}$of square P-FGM plate under uniform load and with a variable-sized Kerr foundation "***de***"(k=2, a/h=10, Kl=20, Ku=20, Ks=20)

4. Conclusions

The present plate theory, the current analytical model, is developed to investigate the bending behavior of simply-supported FG plates subjected to various mechanical loads and resting on different elastic foundations (Winkler–Pasternak and Kerr). Furthermore, virtual displacement is applied to derive the principal equations of equilibrium. These equations are solved numerically using Navier's technique. Subsequently, the results are presented by considering both the inclusion and exclusion of transverse normal strain effects. The non-dimensional deflection, normal stress, and shear stress values, influenced by the side-to-thickness ratio a/h, power law index k, load type, and Winkler–Pasternak (Kw, Kp) and Kerr (Ku, Ks) foundation parameters, are compared and validated against known results in the literature. The results obtained closely resemble those reported by various researchers.

• The highest values of the dimensionless central deflection occur for concentrated loads.

• The lowest values are observed for loads uniformly distributed over 25% of the plate surface.

• In all cases, the non-dimensional central deflection decreases as the thickness ratio increases.

• When an elastic support is present, the shear stress values for the point load approach those observed under uniform loading distribution.

• The highest values of the dimensionless central deflection are noted for the widest foundations across all parameters.

References

Adıyaman, G., Öner, E., Yaylacı, M. and Birinci, A. (2023), "A study on the contact problem of a layer consisting of functionally graded material (FGM) in the presence of body force", *J. Mech. Mater. Struct.*, **18**(1), 125-141. https://doi.org/10.2140/jomms.2023.18.125.

Ameur, M., Tounsi, A., Mechab, I. and El Bedia, A. A. (2011), "A new trigonometric shear deformation theory

for bending analysis of functionally graded plates resting on elastic foundations", *KSCE J. Civil Eng.*, **15**, 1405-1414. https://doi.org/10.1007/s12205-011-1361-z.

Chitour, M., Bouhadra, A., Benguediab, S., Saoudi, A., Menasria, A. and Tounsi, A. (2022), "Effect of Phase Contrast and Geometrical Parameters on Bending Behavior of Sandwich Beams with FG Isotropic Face Sheets", *J. Nano Electr. Phys.*, **14**(5), 05016(6). https://10.21272/jnep.14(5).05016.

Chitour, M., Bouhadra, A., Benguediab, M., Mansouri, K., Menasria, A. and Tounsi, A. (2022), "A new high order theory for buckling temperature analysis of functionally graded sandwich plates resting on elastic foundations", *J. Nano Electr. Phys.*, **14**(3), 03028. https://doi.org/10.21272/jnep.14(3).03028.

Do, N.T. and Pham, Q.H. (2024), "Nonlinear static analysis of functionally graded porous sandwich plates resting on Kerr foundation", *Mech. Adv. Mater. Struct.*, **31**(22), 5678-5691. https://doi.org/10.1080/15376494.2023.2218845.

Faicel, K., Abderahmane, M., Belgacem, M., Abdelhakim, B., Fouad, B., Soumia, B., Abdelouahed, T. (2022), "Thickness stretching and nonlinear hygro-thermo-mechanical loading effects on bending behavior of FG beams", *Struct. Eng. Mech.*, **84**(6), 783-798. https://doi.org/10.12989/sem.2022.84.6.783.

Fuyad, S.T.M., Al Bari, M.A., Makfidunnabi, M., Nain, H.Z., Özdemir, M.E. and Yaylacı, M. (2024), "Finite element analysis of ratcheting on beam under bending-bending loading conditions", *Struct. Eng. Mech.*, **89**(1), 23-31. https://doi.org/10.12989/sem.2024.89.1.023.

Han, J.B. and Liew, K. (1997), "Numerical differential quadrature method for Reissner/Mindlin plates on two-parameter foundations", *Int. J. Mech. Sci.*, **39**(9), 977-989. https://doi.org/10.1016/S0020-7403(97)00001-5.

Himeur, N., Mamen, B., Benguediab, S., Bouhadra, A., Menasria, A., Bouchouicha, B., Benguediab, M. (2022), "Coupled effect of variable Winkler–Pasternak foundations on bending behavior of FG plates exposed to several types of loading", *Steel Compos. Struct.*, **44**(3), 353-369. https://doi.org/10.12989/scs.2022.44.3.353.

Hoang, V.N.V. and Thanh, P.T. (2023), "Influences of arbitrary-distributed Kerr foundation on free vibration and nonlinear transient response of functionally graded plate in thermal environment", *Thin Wall. Struct.*, **188**, 110802. https://doi.org/10.1016/j.tws.2023.110802.

Hoang, V.N.V., Shi, P., Toledo, L. and Vu, H. (2024), "Thermal vibration analysis of FG-GPLRC doubly curved shells partially resting on Kerr foundation based on higher-order shear deformation theory", *Thin Wall. Struct.*, **195**, 111357. https://doi.org/10.1016/j.tws.2023.111357.

Houari, M.S.A., Bessaim, A., Bezzina, S., Tounsi, A., Daikh, A.A., Garg, A. and Belarbi, M.O. (2024), "Thermoelastic bending analysis of thick functionally graded sandwich plates with arbitrary graded material properties using a novel quasi-3D HSDT", *Arch. Civil Mech. Eng.*, **24**(2), 80. https://doi.org/10.1007/s43452-024-00898-6.

Huang, Z., Han, M., Wang, X. and Chu, F. (2023), "Bending analysis of two different types of functionally graded material porous sandwich plates", *Arch. Appl. Mech.*, **93**(8), 3071-3091. https://doi.org/10.1007/s00419-023-02425-0.

Kumar, R., Lal, A., Sutaria, B., Dehury, R.K., Joshi, Y. G. and Gupta, V.S. (2024), "Bending analysis of a porous functionally graded sandwich plate with a hole resting on an elastic foundation", *Acta Mechanica*, **235**, 5061-5078. https://doi.org/10.1007/s00707-024-03989-w.

Li, S.R., Zhang, F. and Liu, R.G. (2024), "Classical and homogenized expressions for the bending solutions of FGM plates based on the four variable plate theories", *Mech. Adv. Mater. Struct.*, **31**(15), 3413-3424. https://doi.org/10.1080/15376494.2023.2177909.

Mekerbi, M., Benyoucef, S., Mahmoudi, A., Tounsi, A., Bousahla, A.A. and Mahmoud, S. (2021), "Thermodynamic behavior of functionally graded sandwich plates resting on different elastic foundation and with various boundary conditions", *J. Sandw. Struct. Mater.*, **23**(3), 1028-1057. https://doi.org/10.1177/1099636219851281.

Meski, K., Boutrid, A., Menasria, A., Bouhadra, A., Mamen, B., Tounsi, A. and Cuong-Le, T. (2024), "Analytical modeling of flexural behavior of advanced composite sandwich beams under nonlinear hygro-thermo-mechanical loads", *Multisc. Multidiscipl. Model. Experim. Des.*, **7**, 4701-4719. https://doi.org/10.1007/s41939-024-00414-6.

Nebab, M., Ait Atmane, H., Bennai, R. and Tounsi, A. (2019), "Effect of variable elastic foundations on static behavior of functionally graded plates using sinusoidal shear deformation", *Arab. J. Geosci.*, **12**(24), 809. https://doi.org/10.1007/s12517-019-4871-5.

Öner, E., Yaylacı, E.U. and Yaylacı, M. (2024), "Multi-method examination of contact mechanics in orthotropic layers under gravity", *Mech. Mater.*, **195**, 105036. https://doi.org/10.1016/j.mechmat.2024.105036.

Park, M. and Choi, D.-H. (2018), "A simplified first-order shear deformation theory for bending, buckling and free vibration analyses of isotropic plates on elastic foundations", *KSCE J. Civil Eng.*, **22**, 1235-1249. https://doi.org/10.1007/s12205-017-1517-6.

Pham, Q.H., Tran, V.K., Tran, T.T., Nguyen, V.C. and Zenkour, A.M. (2023), "Nonlocal higher-order finite element modeling for vibration analysis of viscoelastic orthotropic nanoplates resting on variable viscoelastic foundation", *Compos. Struct.*, **318**, 117067. https://doi.org/10.1016/j.compstruct.2023.117067.

Pham, Q.H., Tran, T.T. and Nguyen, P.C. (2023), "Dynamic response of functionally graded porous-core sandwich plates subjected to blast load using ES-MITC3 element", *Compos. Struct.*, **309**, 116722. https://doi.org/10.1016/j.compstruct.2023.116722.

Pham, Q.H. and Nguyen, P.C. (2022), "Effects of size-dependence on static and free vibration of FGP nanobeams using finite element method based on nonlocal strain gradient theory", *Steel Compos. Struct.*, **45**(3), 331-348. https://doi.org/10.12989/scs.2022.45.3.331.

Pham, Q.H., Tran, V.K. and Nguyen, P.C. (2023), "Nonlocal strain gradient finite element procedure for hygro-thermal vibration analysis of bidirectional functionally graded porous nanobeams", *Waves Random Complex Med.*, 1-32. https://doi.org/10.1080/17455030.2023.2186708.

Rajendran, S., Loganathan, R., Yaylaci, M., Yaylaci, E. U. and Ozdemir, M. E. (2024), "Vibration of piezo-magneto-thermoelastic FG nanobeam submerged in fluid with variable nonlocal parameter", *Adv. Nano Res.*, **16**(5), 489-500. https://doi.org/10.12989/anr.2024.16.5.489.

Rachid, A., Ouinas, D., Lousdad, A., Zaoui, F.Z., Achour, B., Gasmi, H., Tounsi, A. (2022), "Mechanical behavior and free vibration analysis of FG doubly curved shells on elastic foundation via a new modified displacements field model of 2D and quasi-3D HSDTs", *Thin Wall. Struct.*, **172**, 108783. https://doi.org/10.1016/j.tws.2021.108783.

Salehipour, H., Shahmohammadi, M.A. and Civalek, Ö. (2024), "Natural frequencies and modal shapes of folded sandwich plates made of porous core and FG-CNTRC coating layers resting on two parameters elastic foundation", *Aerosp. Sci. Technol.*, **148**, 109077. https://doi.org/10.1016/j.ast.2024.109077.

Sekban, D.M., Yaylacı, E.U., Özdemir, M.E., Öztürk, Ş., Yaylacı, M. and Panda, S.K. (2024), "Formability behavior of AH-32 shipbuilding steel strengthened by friction stir process", *Theor. Appl. Fract. Mech.*, **132**, 104485. https://doi.org/10.1016/j.tafmec.2024.104485.

Sekban, D.M., Yaylacı, E.U., Özdemir, M.E., Yaylacı, M. and Tounsi, A. (2024), "Investigating formability behavior of friction stir-welded high-strength shipbuilding steel using experimental, finite element, and artificial neural network methods", *J. Mater. Eng. Perform.*, 1-9. https://doi.org/10.1007/s11665-024-09501-8.

Sekban, D.M., Yaylaci, E.U., Ozdemir, M.E. and Yaylaci, M. (2024), "Determination of formability behavior of steel used in ships by various methods", *Struct. Eng. Mech.*, ***92***(2), 189-196. https://doi.org/10.12989/sem.2024.92.2.189.

Selvamani, R., Thangamuni, P., Yaylacı, M., Emin Özdemir, M. and Yaylacı, E.U. (2024), "Nonlinear vibration and parametric excitation of magneto-thermo elastic embedded nanobeam using homotopy perturbation technique", *ZAMM J. Appl. Math. Mech.*, **104**(12), e202400525. https://doi.org/10.1002/zamm.202400525.

Selvamani, R., Ebrahimi, F., Yaylacı, M., Öztürk, Ş. and Yaylacı, E.U. (2024), "Nonlinear poro-thermo-forced vibration in curved sandwich magneto-electro-elastic shells under hygrothermal environment", *Acta Mechanica*, **235**(9), 5489-5528. https://doi.org/10.1007/s00707-024-03994-z.

Slimani, R., Menasria, A., Ali Rachedi, M., Mourad, C., Refrafi, S., Nimer, A.A., Mamen, B. (2024), "A novel quasi-3D refined HSDT for static bending analysis of porous functionally graded Plates", *J. Comput. Appl. Mech.*, **55**(3), 519-537. https://10.22059/jcamech.2024.372417.968.

Soltani, M., Momenian, M. and Civalek, O. (2024), "Stability analysis of sandwich double nanobeam-system

with varying cross-section interconnected by Kerr-type three-parameter elastic layer", *Thin Wall. Struct.*, **204**, 112249. https://doi.org/10.1016/j.tws.2024.112249.

Tamrabet, A., Mamen, B., Menasria, A., Bouhadra, A., Tounsi, A., Ghazwani, M.H., Mahmoud, S. (2023), "Buckling behaviors of FG porous sandwich plates with metallic foam cores resting on elastic foundation", *Struct. Eng. Mech.*, **85**(3), 289-304. https://doi.org/10.12989/sem.2023.85.3.289.

Thai, H.T., Park, M. and Choi, D.H. (2013), "A simple refined theory for bending, buckling, and vibration of thick plates resting on elastic foundation", *Int. J. Mech. Sci.*, **73**, 40-52. https://doi.org/10.1016/j.ijmecsci.2013.03.017.

Tran, T.V., Tran, T.-D., Hoa Pham, Q., Nguyen-Thoi, T. and Tran, V.K. (2020), "An ES-MITC3 finite element method based on higher-order shear deformation theory for static and free vibration analyses of FG porous plates reinforced by GPLs", *Math. Probl. Eng.*, **2020**(1), 7520209. https://doi.org/10.1155/2020/7520209.

Nguyen, T.H., Nguyen, T.T., Tran, T.T. and Pham, Q.H. (2023), "Research on the mechanical behaviour of functionally graded porous sandwich plates using a new C1 finite element procedure", *Results Eng.*, **17**, 100817. https://doi.org/10.1016/j.rineng.2022.100817.

Wu, C.P., Chiu, K.H. and Wang, Y.M. (2011), "RMVT-based meshless collocation and element-free Galerkin methods for the quasi-3D analysis of multilayered composite and FGM plates", *Compos. Struct.*, **93**(2), 923-943. https://doi.org/10.1016/j.compstruct.2010.11.015.

Yaghoobi, H. and Fereidoon, A. (2014), "Mechanical and thermal buckling analysis of functionally graded plates resting on elastic foundations: An assessment of a simple refined nth-order shear deformation theory", *Compos. Part B Eng.*, **62**, 54-64. https://doi.org/10.1016/j.compositesb.2014.02.014.

Yaylacı, M., Öner, E., Adıyaman, G., Öztürk, Ş., Uzun Yaylacı, E. and Birinci, A. (2024), "Analyzing of continuous and discontinuous contact problems of a functionally graded layer: theory of elasticity and finite element method", *Mech. Based Des. Struct.*, **52**(8), 5720-5738. https://doi.org/10.1080/15397734.2023.2262562.

Yaylacı, M., Yaylı, M., Öztürk, Ş., Ay, S., Özdemir, M.E., Yaylacı, E.U. and Birinci, A. (2024), "Examining the contact problem of a functionally graded layer supported by an elastic half-plane with the analytical and numerical methods", *Math. Meth. Appl. Sci.*, **47**(12), 10400-10420. https://doi.org/10.1002/mma.10129.

Yaylaci, E.U., Yaylaci, M., Ozdemir, M.E., Terzi, M. and Ozturk, S. (2023), "Analyzing the mechano-bactericidal effect of nano-patterned surfaces by finite element method and verification with artificial neural networks", *Adv. Nano Res.*, **15**(2), 165-174. https://doi.org/10.12989/anr.2023.15.2.165.

Yushan, X. and Zhen, W. (2024), "Non-linear bending analysis and control of graphene-platelets-reinforced porous sandwich plates with piezoelectric layer subjected to electromechanical loading", *Appl. Math. Modell.*, **115708**. https://doi.org/10.1016/j.apm.2024.115708.

Zaoui, F.Z., Ouinas, D. and Tounsi, A. (2019), "New 2D and quasi-3D shear deformation theories for free vibration of functionally graded plates on elastic foundations", *Compos. Part B Eng.*, **159**, 231-247. https://doi.org/10.1016/j.compositesb.2018.09.051.

Zenkour, A., Allam, M. and Radwan, A. (2014), "Effects of transverse shear and normal strains on FG plates resting on elastic foundations under hygro-thermo-mechanical loading", *Int. J. Appl. Mech.*, **6**(5), 1450063. https://doi.org/10.1142/S175882511450063X.

CC